JOURNAL OF GEOPHYSICAL RESEARCH, VOL. 114, C07012, doi:10.1029/2008JC005238, 2009

A threshold for wind-wave growth

Mark A. Donelan[1] and William J. Plant[2]

Received 12 December 2008; revised 24 March 2009; accepted 24 April 2009; published 10 July 2009.

[1] Measurements in a closed, recirculating wind-wave tank using variable wind speeds showed that wind waves in the gravity-capillary range exhibit a threshold in their growth. Surface wave height variance spectral densities in the wave number domain were measured for gravity-capillary waves using both radar backscatter and a wavelet transform technique applied to a laser probe. The measurements showed that when the wind speed was slowly ramped up, a threshold wind speed or friction velocity was required to produce waves. Turning the wind on suddenly showed that the wind stress did not grow as rapidly as the wind since the surface waves supporting the stress grew relatively slowly. Changing water temperature or current in the water caused a pronounced change in the wind speed threshold but not in the friction velocity threshold. Changes in fetch of as much as a factor of 2 had no discernible effect on the thresholds. The results imply that wind speed, being a condition imposed on the air-water interface, causes wave growth, while friction velocity, being a result of air-water interactions, is closely related to surface roughness, hence radar cross section, and changes during wave growth.

Citation: Donelan, M. A., and W. J. Plant (2009), A threshold for wind-wave growth, *J. Geophys. Res.*, *114*, C07012, doi:10.1029/2008JC005238.

1. Introduction

[2] The initial growth of waves by the wind has been studied for many years, both theoretically [*Jeffreys*, 1924, 1925; *Miles*, 1957, 1959a, 1959b, 1960, 1962; *Valenzuela*, 1976; *Riley et al.*, 1982; *Miles*, 1993; *Belcher and Hunt*, 1993; *Cohen and Belcher*, 1999; *Belcher*, 1999] and experimentally [*Shemdin and Hsu*, 1967; *Dobson*, 1971; *Elliott*, 1972; *Snyder*, 1974; *Larson and Wright*, 1975; *Wu et al.*, 1979; *Kawai*, 1979; *Snyder et al.*, 1981; *Plant*, 1982; *Kahma and Donelan*, 1988; *Caulliez et al.*, 1998]. *Donelan and Pierson* [1987] suggested that short wind waves could not grow until the wind exceeded a threshold value at which the energy input from the wind could overcome dissipation due to viscosity. Thus, Donelan and Pierson predicted a very sharp rise from noise levels for short wave spectral densities at low winds. Because of the relationship between these spectral densities and radar cross sections, they therefore predicted that cross sections would also rise sharply from noise levels at low wind speeds. Initial attempts to detect this effect in wind-wave tanks were not successful [*Keller et al.*, 1995] but carefully controlled microwave measurements over the ocean did detect it [*Plant et al.*, 1999a]. In general, the threshold is not pronounced on the ocean owing to variability of the wind, which is especially pronounced at light winds [*Plant*, 2000; *Shankaranarayanan and Donelan*, 2001]. In this paper we report the first observation of this threshold effect in a wind-wave tank at the Canada Centre for Inland Waters (CCIW). Here we will limit ourselves to gravity-capillary waves with wavelengths of 1.51 cm (wave number = 415 rad/m) and 1.88 cm (335 rad/m), Ku band microwave scatterers. Our measurements showed similar behavior for other wind waves, however. We have observed the threshold effect in both microwave backscatter in the tank and in spectral densities obtained from a wavelet transform method applied to laser height/slope measurements made at a single point [*Donelan et al.*, 1996].

[3] The two most commonly used forms for the exponential rate of growth of gravity-capillary wind waves are those given by *Plant* [1982] and *Donelan and Pierson* [1987]. Plant's formulation is

$$\beta = 0.04 u^{*2} \omega / \mathrm{c}^2 \tag{1}$$

where $u*$ is friction velocity or the square root of wind stress divided by air density, c is the phase speed of the growing wave, and ω is its angular frequency. Measurements at CCIW in 1993 using a scanning laser slope gauge [*Uz et al.*, 2003] are in close agreement with the empirical constant 0.04 in (1).

[4] Donelan and Pierson's expression is

$$\beta = \mathrm{K}(\rho_\mathrm{a}/\rho_\mathrm{w})[U(\lambda/2)\mathrm{c} - 1]^2 \omega \tag{2}$$

where K is an empirical constant which Donelan and Pierson determined from the data of *Larson and Wright* [1975] to be 0.194, and $U(\lambda/2)$ is the wind speed at a height above mean water level of one half the wavelength of the growing wind wave. During these experiments, we

[1]Rosenstiel School of Marine and Atmospheric Science, University of Miami, Miami, Florida, USA.
[2]Applied Physics Laboratory, University of Washington, Seattle, Washington, USA.

0148-0227/09/2008JC005238$09.00

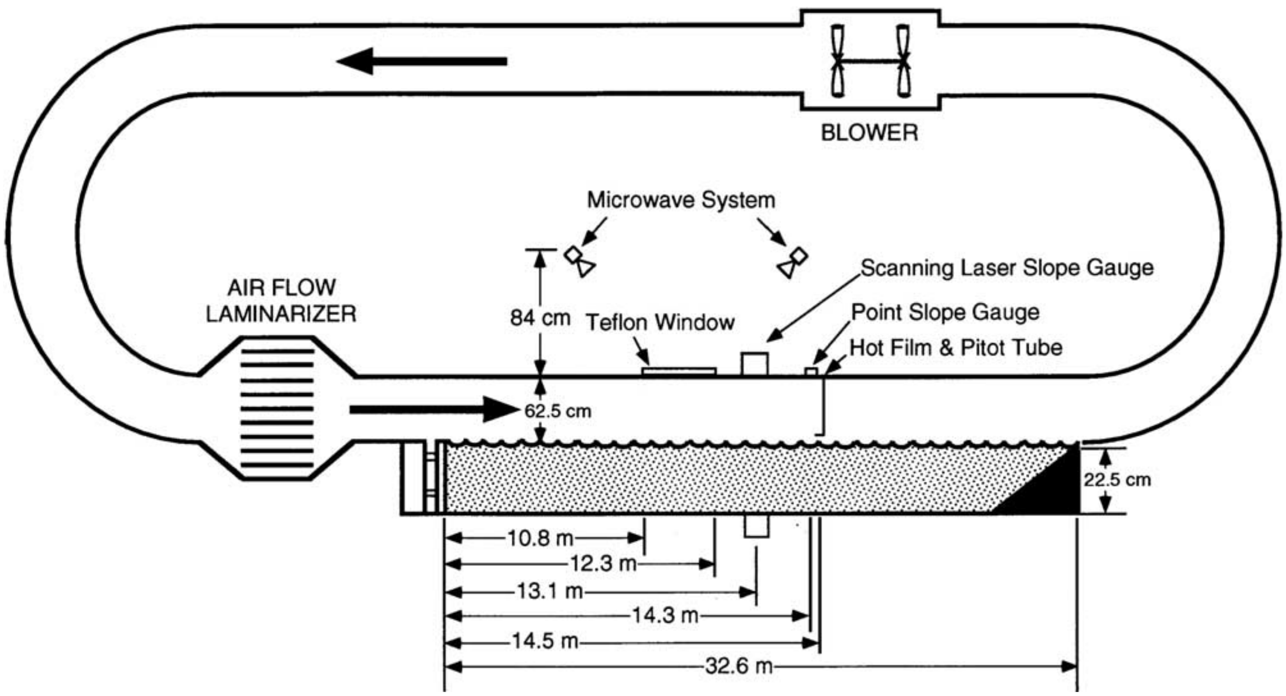

Figure 1. Diagram of the CCIW wind-wave tank showing the placement of instruments.

determined that a better value for K is 0.17 and we will use this value in this paper. $U(\lambda/2)$ is obtained from measurements of U and u^* at other heights z by

$$U(\lambda/2) = U(z) + (u^*/\kappa)\ln(\lambda/(2z)) \quad (3)$$

where κ is von Karman's constant, 0.4. Measured growth rates, β_m, should be less than those given by equations (1) and (2) owing to energy lost to viscous dissipation. Thus,

$$\beta_m = \beta - 4\nu k^2 \quad (4)$$

where k is the wave number of the water wave. The value of β_m is obtained by fitting the increase in spectral density of the water wave to the form $\exp(\beta_m t)$ for times t after a sudden start of the wind.

[5] For wavelengths less than a few tens of centimeters, equations (1) and (2) yield growth rates so close together that it is difficult to distinguish between them by comparison with measured growth rates [*Donelan and Pierson*, 1987]. Here, we attempt to discriminate between them by observing the behavior of the observed threshold wind speed and friction velocity for different water temperatures and currents.

2. Experimental Design

[6] Figure 1 shows the experimental setup. The scanning laser slope gauge shown in Figure 1 was not used in the measurements reported here. Some runs were made with the surface covered for a distance of 5 m, shortening all indicated fetches by this amount. In all cases, care was taken that the airflow made a smooth transition to the water. The microwave antennas were directed both upwind and downwind and were set at incidence angles of 35° and 45°. When the antennas looked upwind, the microwave footprint on the water was at a fetch of 5 or 10 m. Looking downwind, the fetches were 7.4 and 12.5 m. The inside roof and sides of the wind tunnel were lined with microwave absorbing material to a distance of 2.4 m upwind and 1.8 m downwind from the Teflon window. The width of the tank was 76 cm. The wind was either slowly ramped up then down or suddenly started and stopped. Currents up to 30 cm/s could also be set up in the water in the wind direction.

[7] The point height/slope gauge shown in Figure 1 consisted of an Argon-Ion (488 nm–blue) laser transmitting 2 W of power whose beam was directed upward through the water surface. Fluorescein in the water caused the beam, which is blue in air, to fluoresce, producing a green beam (513 nm) in the water. A line-scan camera observing the surface spot from above through the side of the tank tracked the vertical movement of the surface spot. A green filter over the lens discriminated against the blue beam above the water surface. A Fresnel lens and four-quadrant detector above the tank recorded the position of the laser beam after it was refracted by the water surface. The gauge detected all frequencies of motion of the surface up to a maximum determined by the spot size of the beam on the water surface and by the sampling frequency, which was 1000 Hz for the measurements reported here. However, signal-to-noise problems in fact limit the frequency response to a value somewhat lower than this. The spot size was about 1 mm, so wave numbers up to about 3000 rad/m could be measured. The maximum slope that could be measured by the system was 42°. As outlined in more detail below, complete wave height variance spectra as a function of wave number and frequency, $F(\mathbf{k}, \omega)$, could be obtained from this gauge after processing.

[8] The microwave system was identical to that described in detail by *Plant et al.* [1994] except that the frequency had

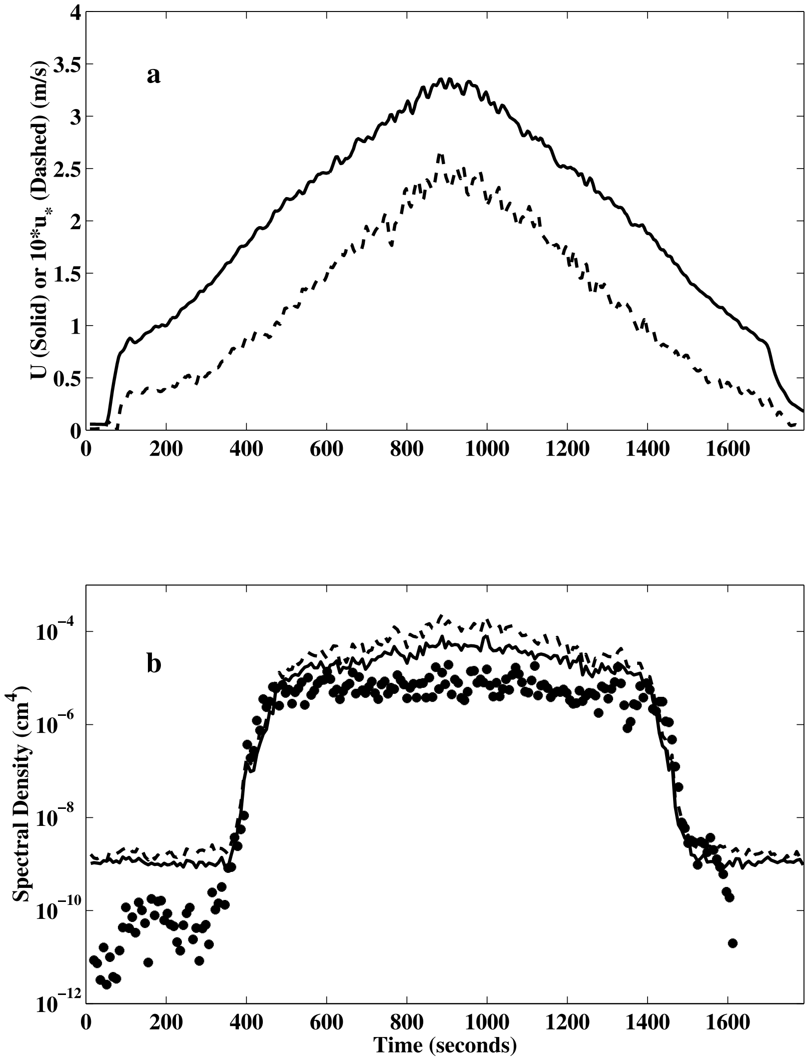

Figure 2. (a) Time plot of wind speed at 3 cm (solid line) and friction velocity at the surface (dashed line) for a slowly ramped wind (ramp rate is 0.34 cm/s/s). (b) Time plot of $F(k_b, 0)$ from Ku band radar cross sections and $F(k_b, 0)$ from the laser height/slope gauge, where k_b = 335 rad/m. The radar antenna was at a 35° incidence angle looking upwind. The fetch at the radar footprint was 10.0 m, while the fetch was 14.3 m to the laser probe. Solid curve, radar, VV; dashed curve, radar, HH; dots, laser.

been shifted up to Ku band; it is exactly the same system used by *Plant et al.* [1999b]. Briefly, the system was a coherent, dual-polarized, continuous wave system and data were collected on horizontal transmit/horizontal receive (HH) and vertical transmit/vertical receive (VV) polarizations simultaneously. Exact frequencies were 14.00 GHz for VV and 14.06 for HH. One-way half-power antenna beam widths were 6.6° in the E plane and 5.0° in the H plane, and the beam viewed the water surface through a 6 mm thick Teflon window. The height of the antennas was maintained at 147 cm above mean water level for all incidence angles and look directions. Calibration procedures differed slightly from those described by *Plant et al.* [1994] owing to the laboratory setting. Water was drained from the tank, and a corner reflector was placed on absorbing material on the bottom of the tank at various positions in the beam. Return from the corner reflector was measured as a function of position in the beam and used to calculate calibration constants and illuminated areas as described by *Plant et al.* [1994]. Microwave return was collected at a sample rate of 257 Hz to fill an array 1024 samples long in 4 s during the ramped runs. In the sudden start runs, the sample rate was 1042 Hz for the same array size, yielding a measurement every 0.98 s. This array was then Fourier transformed to produce Doppler spectra that were stored on optical disks. A reference signal from the microwave system and the mean value of the sum of the squares of the in phase and quadrature channels were stored for later use in computing normalized radar cross sections, σ_o.

[9] Winds in the tank were measured using a Pitot tube and hot X-film anemometers, from which friction velocities could be calculated. The height of the Pitot tube varied from 3 to 8.1 cm above the water surface during the experiments, and the hot film was 3.2 cm directly above the Pitot tube. The Pitot tube was used to calibrate the X-film anemometers several times per day by ramping the wind speed up and down. The X-film anemometers were then used to determine the horizontal mean wind speed and fluctuations

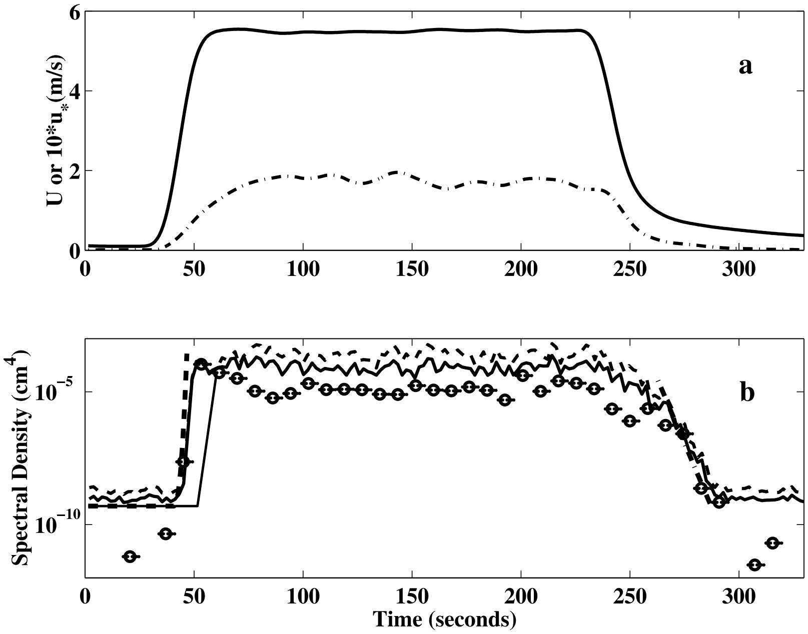

Figure 3. (a) Time plot of wind speed at 4.7 cm and friction velocity for a suddenly started and stopped wind. Solid line, wind speed; dash-dotted line, friction velocity times 10. (b) Time plot of $F(k_b, 0)$ from Ku band radar cross sections and $F(k_b, 0)$ from laser height/slope gauge for k_b = 335 rad/m. The radar antenna was directed upwind at a 35° incidence angle. Solid curve, radar, VV; dashed curve, radar, HH; circles (error bars indicate integration time), laser; solid line, exponential wave growth with Plant's growth rate, equation (1) using the equilibrium friction velocity; dashed line, wave growth from exponential wave growth with Donelan and Pierson's growth rate, equation (2) using the time-varying wind speed; dash-dotted line, exponential decay due to viscosity.

of both horizontal and vertical components of the wind. From these the friction velocity at the height (usually 6.2 cm) of the X-film anemometers $u^*(z)$ was calculated. Wind speeds shown in Figures 4–6 have been adjusted to be those at a 3 cm height; in Figures 2 and 3 measured wind speeds are shown. Friction velocities quoted here have been corrected to be those at the surface. The experimentally determined correction was

$$u^{*2}(0) = [25/(25 - z)]u^{*2}(z) \quad (5)$$

where z is the height of the measurement in cm [*Uz et al.*, 2002]. Note that the change of u^* is small in the region below 6 cm, so that a constant flux approximation is appropriate in deducing the velocity profile at lower heights. Air and water temperatures were recorded during each run, and the water surface was skimmed free of surfactants each morning before the runs began. The wind measurements were recorded on a different computer from the radar measurements. However, a synchronizing signal, a 30 s saw tooth, was recorded on both computers as was the signal from the Pitot tube. The Pitot tube signals recorded on the two computers were plotted together to verify synchronization. As noted above, winds were varied in two ways. In the mode we call "ramped," the wind speed was slowly increased linearly to a maximum value then slowly decreased linearly at the same rate. The rate at which the wind speed was changed was 0.34 cm/s in one second. Thus it required 294 s for the wind to change by 1 m/s so the waves remained in equilibrium with the wind in this mode. We could have performed this part of the study by stepping the winds through a series of fixed values. The threshold discussed below was so sharp, however, that this method could have missed it. The second mode we call the "sudden start" mode. Here the fan was turned on suddenly and held at a constant speed until it was turned off. The wind speed had a risetime that will be shown in Figures 2 and 3 but was generally near equilibrium by the time waves began to grow.

3. Wave Number Spectra

[10] Along with wind speed and friction velocity, the wave height variance spectrum as a function of wave number, $F(k_x, k_y)$ where k_x is the along-tank wave number and k_y is the cross-tank wave number, was central to this study. We measured $F(k_x, k_y)$ using both radar backscatter and a wavelet technique applied to the output of the laser gauge.

[11] At sufficiently low wind speeds, radar backscatter from rough water surfaces is Bragg scattering. Under these circumstances, the relationship between the radar cross section, σ_o, and $F(k_x, k_y)$ is given by

$$F(k_b, 0) = \sigma_o / \left(16\pi k_o^4 \cos\theta_i |g_{pq}|^2\right) \quad (6)$$

where

$$k_b = 2k_o \sin\theta_i, \quad (7)$$

g_{pq} is a function of incidence angle and dielectric constant depending on polarization, (p, q), θ_i is incidence angle, and k_o is the wave number of the microwave radiation. Expressions for g_{pq} are given by *Plant* [1990].

[12] This expression does not work well at higher wind speeds where the more complex composite surface scattering theory must be used. Our concern in this paper, however, is primarily with the growth of wind waves near the threshold wind speed, which is low. Thus we always relate spectral density F to cross section σ_o by equation (6) in this paper.

[13] Radar backscatter yields $F(k_x, k_y)$ only for a very small range of wave numbers around ($2k_o \sin\theta_i$, 0), the Bragg wave number. By contrast, a wavelet technique developed by *Donelan et al.* [1996] yields F for all values of (k_x, k_y). In these experiments, this technique was applied to height/slope measurements made by the laser at a single point by expanding the surface displacement in a Taylor series about the point of measurement. Given the slopes in the along- and cross-tank directions, the first two terms in the series may be evaluated, effectively yielding wave amplitude measurements at four points, two in each the along- and cross-tank directions. To ensure that the effect of curvature and higher-order terms is relatively small, the separation of these virtual probes from the location of the height measurement needs to be small. We set this separation to 0.01 mm. Comparisons with duplicate runs using a separation of 0.05 mm showed no perceptible difference. Applying wavelet techniques to the outputs of these four virtual probes then yields time series of wave heights in various, nonoverlapping frequency bands. Phase differences, $\Delta\varphi_i$, and separations, $\mathbf{r_i} = (r_i, \alpha_i)$, between pairs of probes at 90° to each other then yield the instantaneous wave number, k, and direction, φ_i, associated with each frequency according to the following equations:

$$k = (r_2 \Delta\varphi_1 \sin\alpha_2 - r_1 \Delta\varphi_2 \sin\alpha_1)/(r_1 r_2 \sin(\alpha_2 - \alpha_1)\cos\varphi) \tag{8}$$

$$\varphi = \tan^{-1}[(r_2\Delta\varphi_1 \cos\alpha_2 - r_1\Delta\varphi_2\cos\alpha_1) / (r_1\Delta\varphi_2 \sin\alpha_1 - r_2\Delta\varphi_1 \sin\alpha_2)] \tag{9}$$

[14] Taking the squared magnitude of the wave amplitude in each frequency band and averaging many such individual measurements yields the wave height variance spectrum as a function of wave number for each frequency band. That is, it yields the complete variance spectrum of the wave height as a function of (k_x, k_y, ω) where ω is angular frequency. Integration over ω then yields $F(k_x, k_y)$.

4. Observations of a Threshold

[15] Figure 2 shows the result of slowly ramping the wind speed up and then down. As stated above, the ramp speed was sufficiently slow that the waves were always essentially in equilibrium. A pronounced threshold is apparent in the growth of the wind wave spectral densities shown in Figure 2b. This threshold occurs at the point where the growth rate β as given by either equation (1) or (2) is equal to the rate of viscous dissipation, $4\nu k^2$. Note that spectral densities measured by the radar and laser agree very well in the threshold regions, although the laser has a somewhat lower noise level.

[16] The situation is somewhat different if the wind is suddenly started and stopped as shown in Figure 3. Figure 3a shows that the friction velocity increases at a much slower rate than the wind owing to the relatively slow growth of the surface waves that support the wind stress. Because of this slow growth of the stress, gravity-capillary wind waves do not grow in a constant stress environment as usually assumed theoretically. As both the radar and laser response demonstrate, the short waves investigated here grow more rapidly than the wind stress. Donelan and Pierson's formulation, based on the time-varying wind at a height of half the wavelength, provides a good prediction of wave growth. Plant's formulation using the equilibrium friction velocity cannot yield a starting time for this growth.

[17] Two comments relating to these observations should be made at this point. First, the slow growth of the friction velocity is due to the fact that wind stress is supported by all waves on the surface and longer waves than those observed here grow more slowly [*Plant*, 1982]. Second, once the wind stress has risen to its equilibrium value, Plant's growth rate is nearly the same as that of Donelan and Pierson as noted previously so that both predict the same energy input from the wind.

5. Factors Affecting the Threshold

[18] To see if wave propagation down the tank might play a role in the location of the threshold, we measured radar cross sections as a function of wind speed and friction velocity at a wave number of 415 rad/m and a variety of fetches. This variety is possible because we have combined upwind and downwind radar looks, with and without the water surface mask, with the laser data. Figure 4 shows the results for a wind speed increasing at 0.3 cm/s/s. Clearly, the threshold wind speed, friction velocity, and the wave height spectral densities at higher wind speeds are independent of fetch.

[19] We next examined the effect of a change in water temperature on the threshold wind speeds and friction velocities. Figure 5a shows that the threshold friction velocity does not depend on water temperature but that the threshold wind speed does. We interpret this to mean that the wind speed controls the rate of growth of wind waves and that the friction velocity adjusts to changes in the water surface. We believe these results to be very significant for air-sea interactions and microwave scatterometry.

[20] The reasoning behind these conclusions is as follows. If the growth rate, β, of wind waves depends on the wind speed near the surface as equation (2) states, then it will not change with water temperature for any given wind speed. But if the water temperature is increased, the viscosity will decrease resulting in lower viscous dissipation, $4\nu k^2$. By equation (4), then, a lower wind speed will result in $\beta_m = 0$. That is the threshold will occur at lower wind speeds at higher water temperatures if energy input from wind to waves is controlled by wind speed. This is what we observe. The expected change in the wind speed threshold can be easily computed from equations (2), (3), and (4) by finding $U(\lambda/2)$ where $\beta_m = 0$. For a change in kinematic

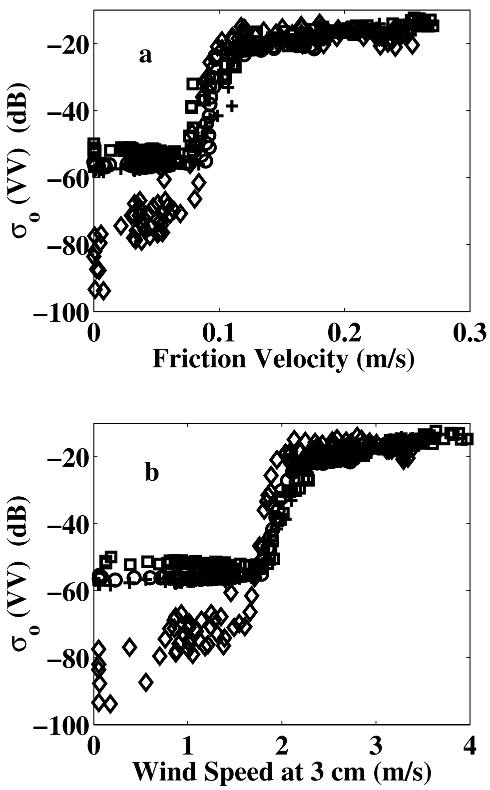

Figure 4. Ku band cross sections, σ_o, at different fetches for a slowly increasing wind versus (a) friction velocity and (b) wind speed at 3 cm. Rate of change of wind speed is 0.3 cm/s/s. Symbols are as follows: squares, σ_o (VV), downwind, 7.4 m fetch; pluses, σ_o (VV), upwind, 10.0 m fetch; circles = σ_o (VV), downwind, 12.4 m fetch; diamonds, spectral densities from laser converted to σ_o (VV), 14.3 m fetch. Radar is at a 45° incidence angle; k_b = 415 rad/m.

viscosity ν from 0.0100 cm^2/s at 20°C to 0.0081 cm^2/s at 29.4°C, we find an increase in the wind speed threshold of 0.18 m/s. This agrees well with the 0.2 m/s change shown in Figure 5. We have also taken into account the change in air and water densities although these have little effect.

[21] On the other hand, Figure 3 suggests that friction velocity adjusts to surface conditions. In fact, Figure 3 says that friction velocity is lower when the waves are lower. But at higher water temperatures, the threshold is shifted to lower wind speeds so waves at these wind speeds are higher than at lower water temperatures. The friction velocity therefore becomes higher at these wind speeds. The data indicate that this causes the friction velocity threshold to remain constant. Since radar backscatter responds to surface wave intensities, this means that the backscatter is more closely related to wind stress than to wind speed.

[22] This latter statement requires a bit of qualification. Wind stress consists of the sum of two parts: skin stress and form stress. The latter component is supported by all the waves moving relative to the wind, i.e., the entire slope-spectrum weighted by the square of the velocity difference between waves and wind [*Donelan*, 1998]. On the other hand equations (6) and (7) show that σ_o depends on surface waves only in a restricted range of wave numbers. Thus the relationship between σ_o and friction velocity will be broken if the wave spectrum is not self-similar. This requires that all wave components in the spectrum respond similarly to the wind speed when they are in equilibrium. This condition corresponds to a pure wind sea. By contrast, the relationship between σ_o and stress is not expected to apply in the presence of swell.

[23] The changes in the threshold wind speed and friction velocity caused by changes in current are illustrated in Figure 6. Here again we look at the decreasing part of the wind speed ramp. We plot radar cross section at a 45° incidence angle (Bragg wave number = 415 rad/m) versus either wind speed or friction velocity for currents of 0, 12, and 27.6 cm/s in the same direction as the wind. Increasing the current clearly increases the threshold wind speed but changes the threshold friction velocity little. The increased wind speed threshold, however, is larger than the currents used: going from zero current to 12 cm/s increases the threshold by 41 cm/s while going from 0 to 27.6 cm/s increases it by 59 cm/s. If the current were laminar, one would expect that wave growth would occur whenever the wind relative to the moving water exceeded the constant threshold. Thus the threshold in the laboratory reference frame would increase by the amount of the current. But the current is obviously turbulent as evidenced by the increase

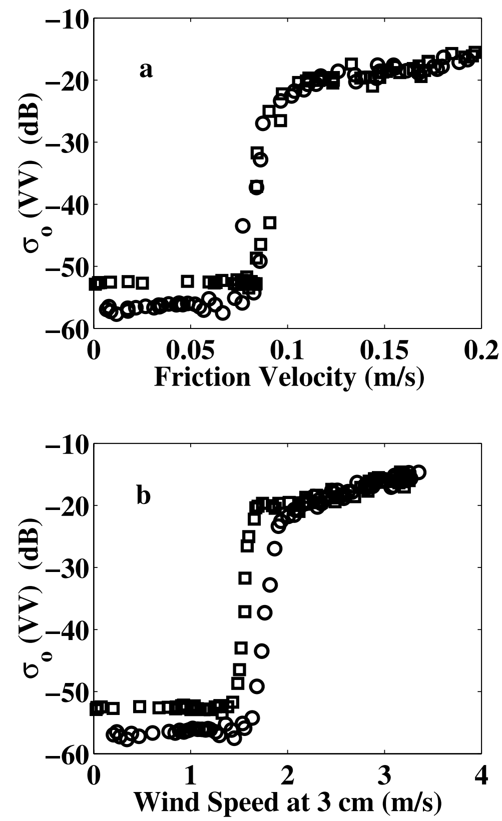

Figure 5. Ku band radar cross sections, σ_o, at two different water temperatures for a wind decreasing at 0.3 cm/s/s versus (a) friction velocity and (b) wind speed at 3 cm. Data taken at a fetch of 10.0 m with an upwind look direction; incidence angle is 45° (k_b = 415 rad/m). Rate of change of wind speed is 0.3 cm/s/s. Air temperatures were between 20°C and 22°C. Symbols indicate water temperature as follows: circles, 20.0°C; squares, 29.4°C.

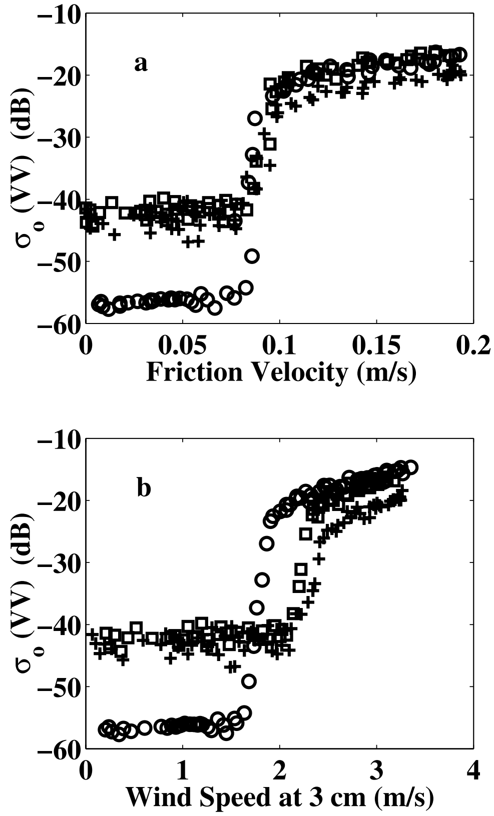

Figure 6. Ku band radar cross sections, σ_o, with different currents and a decreasing wind versus (a) friction velocity and (b) wind speed at 3 cm. Rate of change of wind speed was near 0.3 cm/s/s, air temperatures were about 22°C, and water temperatures were between 18°C and 21°C. Symbols indicate different currents as follows: circles, 0 cm/s, squares, 12 cm/s, pluses, 27.6 cm/s. The antenna was directed upwind for the two lower currents (fetch = 10.0 m) and downwind (with mask) for the higher (fetch = 7.4 m); the incidence angle was 45°C (k_b = 415 rad/m).

in cross section below the threshold. The fact that the threshold increases more than expected when starting from zero current suggests that the eddy viscosity associated with this turbulence increases the dissipation of the waves. Thus a larger wind speed relative to the moving water surface is required to maintain waves than would be required in the absence of turbulence. The slight decrease in spectral density above the threshold wind speed also supports the idea of turbulent damping. Small amounts of turbulence are required to generate the initial roughness but increasing the level of turbulence increases the dissipation [see *Veron and Melville*, 2001], causing short waves to be damped. These measurements clearly show that a given level of radar cross section will be related to a different wind speed depending on the current in the water. The relationship between radar cross section and wind stress appears to be little affected by currents, however.

6. Conclusion

[24] Properties of wind-generated gravity-capillary waves have been studied. Spectral densities of these waves during their initial growth have been derived from microwave backscattering cross sections and from a wavelet method applied to laser height and slope measurements at a single point. The two methods agree very well and both show that a threshold wind speed or friction velocity exists below which the waves cannot grow. The reason is clearly that energy input from the wind does not exceed viscous dissipation below this threshold. The threshold values of wind speed or friction velocity have been shown to be independent of fetch in the tank when the fetch is changed by a factor of 2. The wind speed threshold has been shown to decrease when the water temperature is increased but the friction velocity threshold does not depend on water temperature. Similarly the wind speed threshold increases when currents in the same direction as the wind exist in the water but the friction velocity threshold remains constant. Furthermore, the friction velocity has been shown to increase more slowly than the wind speed when the wind is suddenly started. Thus the initial growth of gravity-capillary waves is not in a constant-stress environment as most theories presume. We conclude from these measurements that wind speed just above the water controls the growth of these short waves while the friction velocity adjusts to surface roughness and therefore is more correlated with radar backscatter when the stress is supported primarily by these short slow moving waves.

[25] **Acknowledgments.** The authors would like to thank Bill Keller, Ken Hayes, and Vahid Hesany for their help in carrying out these experiments. They would also like to thank the staff of the National Water Research Institute, in particular, D.C. Beesley, who operated the wind-wave tank. The project was funded by NSF grant OCE 9402852AM01 and ONR grants N00014-93-1-0016 and N00014-00-1-0075.

References

Belcher, S. E. (1999), Wave growth by non-separated sheltering, *Eur. J. Mech. B Fluids*, *18*(3), 447–462, doi:10.1016/S0997-7546(99)80041-7.
Belcher, S. E., and J. C. R. Hunt (1993), Turbulent shear-flow over slowly moving waves, *J. Fluid Mech.*, *251*, 109–148, doi:10.1017/S0022112093003350.
Caulliez, G., N. Ricci, and R. Dupont (1998), The generation of the first visible wind waves, *Phys. Fluids*, *10*, 757–759, doi:10.1063/1.869600.
Cohen, J. E., and S. E. Belcher (1999), Turbulent shear flow over fast-moving waves, *J. Fluid Mech.*, *386*, 345–371, doi:10.1017/S0022112099004383.
Dobson, F. W. (1971), Measurements of atmospheric pressure on wind-generated sea waves, *J. Fluid Mech.*, *48*(1), 91–127, doi:10.1017/S0022112071001496.
Donelan, M. A. (1998), Air-water exchange processes, in *Physical Processes in Lakes and Oceans*, *Coastal Estuarine Stud.*, vol. 54, edited by J. Imberger, pp. 19–36, AGU, Washington, D. C.
Donelan, M. A., and W. J. Pierson Jr. (1987), Radar scattering and equilibrium ranges in wind-generated waves with application to scatterometry, *J. Geophys. Res.*, *92*(C5), 4971–5029, doi:10.1029/JC092iC05p04971.
Donelan, M. A., W. M. Drennan, and A. K. Magnusson (1996), Nonstationary analysis of the directional properties of propagating waves, *J. Phys. Oceanogr.*, *26*(9), 1901–1914, doi:10.1175/1520-0485(1996)026<1901:NAOTDP>2.0.CO;2.
Elliott, J. A. (1972), Microscale pressure fluctuations near waves being generated by the wind, *J. Fluid Mech.*, *54*(3), 427–448.
Jeffreys, H. (1924), On the formation of waves by wind, *Proc. R. Soc. London, Ser. A.*, *107*, 189–206.
Jeffreys, H. (1925), On the formation of waves by wind II, *Proc. R. Soc. London, Ser.A*, *110*, 341–347.
Kahma, K. K., and M. A. Donelan (1988), A laboratory study of the minimum wind-speed for wind wave generation, *J. Fluid Mech.*, *192*, 339–364, doi:10.1017/S0022112088001892.
Kawai, S. (1979), Generation of initial wavelets by instability of a coupled shear flow and their evolution to wind waves, *J. Fluid Mech.*, *93*(4), 661–703, doi:10.1017/S002211207900197X.

Keller, M. R., B. L. Gotwols, W. J. Plant, and W. C. Keller (1995), Comparison of optically derived spectral densities and microwave cross sections in a wind-wave tank, *J. Geophys. Res.*, *100*(C8), 16,163–16,178, doi:10.1029/95JC00688.

Larson, T. R., and J. W. Wright (1975), Wind-generated gravity-capillary waves: Laboratory measurements of temporal growth rates using microwave backscatter, *J. Fluid Mech.*, *97*, 455–479.

Miles, J. W. (1957), On the generation of surface waves by shear flows, *J. Fluid Mech.*, *3*, 185–204, doi:10.1017/S0022112057000567.

Miles, J. W. (1959a), On the generation of surface waves by shear flows, Part 2, *J. Fluid Mech.*, *6*, 568–582, doi:10.1017/S0022112059000830.

Miles, J. W. (1959b), On the generation of surface waves by shear flows, Part 3, *J. Fluid Mech.*, *6*, 583–598, doi:10.1017/S0022112059000842.

Miles, J. W. (1960), On the generation of surface waves by turbulent shear flows, *J. Fluid Mech.*, *7*, 469–478, doi:10.1017/S0022112060000220.

Miles, J. W. (1962), On the generation of surface waves by shear flows. Part 4, *J. Fluid Mech.*, *13*, 433–448, doi:10.1017/S0022112062000828.

Miles, J. W. (1993), Surface-wave generation revisited, *J. Fluid Mech.*, *256*, 427–441, doi:10.1017/S0022112093002836.

Plant, W. J. (1982), A relationship between wind stress and wave slope, *J. Geophys. Res.*, *87*(C3), 1961–1967, doi:10.1029/JC087iC03p01961.

Plant, W. J. (1990), Bragg scattering of electromagnetic waves from the air/sea interface, in *Surface Waves and Fluxes: Current Theory and Remote Sensing*, vol. 2, edited by G. L. Geernaert and W. J. Plant, pp. 41–108, Kluwer Acad., Norwell, Mass.

Plant, W. J. (2000), Effects of wind variability on scatterometry at low wind speeds, *J. Geophys. Res.*, *105*(C7), 16,899–16,910, doi:10.1029/2000JC900043.

Plant, W. J., W. C. Keller, R. A. Petitt, and E. A. Terray (1994), The dependence of microwave backscatter from the sea on illuminated area: Correlation times and lengths, *J. Geophys. Res.*, *99*(C5), 9705–9723, doi:10.1029/93JC00862.

Plant, W. J., D. E. Weissman, W. C. Keller, V. Hesany, K. Hayes, and K. W. Hoppel (1999a), Air/sea momentum transfer and the microwave cross section of the sea, *J. Geophys. Res.*, *104*(C5), 11,173–11,191, doi:10.1029/1999JC900038.

Plant, W. J., W. C. Keller, V. Hesany, T. Hara, E. Bock, and M. Donelan (1999b), Bound waves and Bragg scattering in a wind-wave tank, *J. Geophys. Res.*, *104*(C2), 3243–3263, doi:10.1029/1998JC900061.

Riley, D. S., M. A. Donelan, and W. H. Hui (1982), An extended Miles' theory for wave generation by wind, *Boundary Layer Meteorol.*, *22*, 209–225, doi:10.1007/BF00118254.

Shankaranarayanan, K., and M. A. Donelan (2001), A probabilistic approach to scatterometer model function verification, *J. Geophys. Res.*, *106*(C9), 19,969–19,990, doi:10.1029/1999JC000189.

Shemdin, O. H., and E. Y. Hsu (1967), Direct measurement of aerodynamic pressure above a simple progressive gravity wave, *J. Fluid Mech.*, *30*(pt. 2), 403–416, doi:10.1017/S0022112067001508.

Snyder, R. L. (1974), A field study of wave-induced pressure fluctuations above surface gravity waves, *J. Mar. Res.*, *32*(3), 497–531.

Snyder, R. L., F. W. Dobson, J. A. Elliott, and R. B. Long (1981), Array measurements of atmospheric pressure fluctuations above surface gravity waves, *J. Fluid Mech.*, *102*, 1–59, doi:10.1017/S0022112081002528.

Uz, B. M., M. A. Donelan, T. Hara, and E. J. Bock (2002), Laboratory studies of wind stress over surface waves, *Boundary Layer Meteorol.*, *102*, 301–331, doi:10.1023/A:1013119313063.

Uz, B. M., T. Hara, E. J. Bock, and M. A. Donelan (2003), Laboratory observations of gravity-capillary under transient wind forcing, *J. Geophys. Res.*, *108*(C2), 3050, doi:10.1029/2000JC000643.

Valenzuela, G. R. (1976), The growth of gravity-capillary waves in a coupled shear flow, *J. Fluid Mech.*, *76*, 229–250, doi:10.1017/S0022112076000608.

Veron, F., and W. K. Melville (2001), Experiments on the stability and transition of wind-driven water surfaces, *J. Fluid Mech.*, *446*, 25–65.

Wu, H. Y., E. Y. Hsu, and R. L. Street (1979), Experimental study of nonlinear wave-wave interaction and white-cap dissipation of wind-generated waves, *Dyn. Atmos. Oceans*, *3*, 55–78, doi:10.1016/0377-0265(79)90037-X.

M. A. Donelan, Rosenstiel School of Marine and Atmospheric Science, University of Miami, Miami, FL 33149-1098, USA. (mdonelan@rsmas.miami.edu)

W. J. Plant, Applied Physics Laboratory, University of Washington, Seattle, WA 98105-6698, USA.